Rapid Oxidation of Arsenite in a Hot Spring Ecosystem, Yellowstone National Park

HEIKO W. LANGNER, COLIN R. JACKSON, TIMOTHY R. MCDERMOTT, AND WILLIAM P. INSKEEP*

Thermal Biology Institute and Department of Land Resources and Environmental Sciences, Montana State University– Bozeman, Bozeman, Montana 59717-3120

Geothermal springs within Yellowstone National Park (YNP) often contain arsenic (As) at concentrations of 10– 40 μM, levels that are considered toxic to many organisms. Arsenite (As(III)) is often the predominant valence state at the point of discharge but is rapidly oxidized to arsenate (As(V)) during transport in shallow surface water. The current study was designed to establish rates and possible mechanisms of As(III) oxidation and to characterize the geochemical environment associated with predominant microbial mats in a representative acid–sulfate–chloride (pH 3.1) thermal (58–62 °C) spring in Norris Basin, YNP. At the spring origin, total soluble As was predominantly As(III) at concentrations of 33 μM. No oxidation of As(III) was detected over the first 2.7 m downstream from the spring source, corresponding to an area dominated by a yellow filamentous S^0-rich microbial mat. However, rapid oxidation of As(III) to As(V) was observed between 2.7 and 5.6 m, corresponding to termination of the S^0-rich mats, decreases in dissolved sulfide, and commencement of a brown Fe/As-rich mat. Rates of As(III) oxidation were estimated, yielding an apparent first-order rate constant of 1.2 min^{-1} (half-life = 0.58 min). The oxidation of As(III) was shown to require live organisms present just prior to and within the Fe/As-rich mat. Complementary analytical tools used to characterize the brown mat revealed an As:Fe molar ratio of 0.7 and suggested that this filamentous microbial mat contains iron(III) oxyhydroxide coprecipitated with As(V). Results from the current work are the first to provide a comprehensive characterization of microbially mediated As(III) oxidation and the geochemical environments associated with microbial mats in acid– sulfate–chloride springs of YNP.

Introduction

Geothermal springs provide unique environments for the evolution and establishment of microbial communities. Besides adaptation to elevated temperatures, microorganisms inhabiting such environments must cope with a variety of extreme chemical conditions such as low pH and high concentrations of toxic elements. For example, concentrations of arsenic in geothermal springs of Yellowstone National Park (YNP), Wyoming, commonly range from 10 to 40 μM (*1, 2*), but we have measured concentrations as high as 2 mM

* Corresponding author phone: (406)994-5077; fax: (406)994-3933; e-mail: binskeep@montana.edu.

in certain S-rich thermal springs. Microorganisms living in these environments have evolved mechanisms to endure the toxic effects of As. In nonthermal environments, some bacteria have been found to utilize arsenite (As(III)) as an energy source (*3, 4*) or arsenate (As(V)) as an electron acceptor during anaerobic respiration (*5*). Known mechanisms of As detoxification involve the reduction of As(V) to As(III) followed by the active transport of As(III) out of the cell (*6*). Highly toxic As(III) may also be converted to less toxic forms such as As(V) or methylated forms of As (*7, 8*).

Previous studies of thermal springs in YNP have shown that As is often discharged as As(III) (*1, 9, 10*), and the ratio of As(V):As(III) upon discharge may reflect the degree to which the geothermal water was preexposed to oxygenated conditions. In springs where As(III) is the dominant species in the source water, the amount of As(V) increases over short stream intervals such that the larger drainages are often dominated by As(V) (*1, 9, 10*). These results support the conclusion that significant oxidation of aqueous As(III) occurs via chemical or biological processes after discharge from the source. Stauffer et al. (*10*) showed that As(III) was conserved after discharge from an 89 °C spring source until the stream temperature declined to 45–63 °C, but further downstream, where the temperature had decreased to 33–41 °C, 50% of the As(III) was oxidized to As(V). Wilkie and Hering (*11*) reported rapid oxidation of As(III) in a stream subject to inputs of thermal waters originating in the Sierra Nevada Mountains, corresponding to an As(III) half-life of approximately 0.3 h. They provided evidence that microbial populations colonizing the surface of aquatic macrophytes were essential for the oxidation of As(III). Given that the abiotic oxidation of As(III) in natural environments appears to be relatively slow (*12, 13*), it is likely that the observed oxidation in acidic hot springs of YNP is also microbially mediated. If this is the case, As(III) oxidation may occur as a result of detoxification pathways (*7, 8*) or due to chemo-lithoautotrophic growth by organisms capable of coupling the oxidation of As(III) to As(V) with the fixation of inorganic carbon (*3, 4*).

Although previous results (*1, 9–11*) have documented the oxidation of As(III) in thermal springs of YNP, no studies have reported details regarding the rates and possible contributing mechanisms of As(III) oxidation in acidic hot springs of YNP. Consequently, the objectives of this study were to (i) determine rates of As(III) oxidation in one representative acidic hot spring in Norris Basin, YNP, and to inventory the geochemical conditions that may influence both As(III) oxidation and associated microbial communities; (ii) evaluate potential biotic and abiotic contributions controlling As(III) oxidation in the spring; and (iii) characterize the geochemical environment of the predominant microbial mats colonizing the thermal spring. This paper accompanies a collaborative effort by Jackson et al. (*14*) to identify the predominant microbial populations associated with the microbial mats described here, utilizing cultivation-independent molecular methods and phylogenetic analyses.

Materials and Methods

Aqueous Chemistry. The thermal spring selected for this study (44°43′54.8″ N, 110°42′39.9″ W, Spring No. NHSP106, thermal inventory of YNP) is typical of many springs found in the Hundred Springs Plain of Norris Geyser Basin. The spring was selected after preliminary analyses in October 1999 that showed rapid oxidation of As(III) upon discharge. This spring discharges water between 58 and 63 °C (observed over a 1-yr period) and exhibits a distinctive sequence of

sample locations visual features	temp (°C)	distance (m)	travel time[a] (min)	velocity[b] (m min^{-1})	As(V): As(ts)[c]
spring source	63	0	0		<0.06
yellow mat	60	1.7	0.33	5.2	<0.06
yellow mat end	58	2.7	0.47	7.1	<0.06
no mat	55	3.7	0.55	12.5	0.09
brown mat start	54	4.4	0.67	5.8	0.16
brown mat	51	5.0	0.82	4.0	0.29
transition brown-green	49	5.3	0.92	3.0	0.38
green mat	46	5.6	1.02	3.0	0.45

[a] Determined by timing suspended particulates in the spring that had been loosened from the spring bottom. [b] Calculated for the interval preceding the respective sampling location. [c] Average ratios of As(V): As(ts); total soluble arsenic (As(ts)) = 33 μM throughout spring sampling interval.

well-separated microbial mats covering the spring floor in both longitudinal and lateral directions. The data presented in this paper were collected during four field trips on November 16, 1999; January 26, 2000; June 6, 2000; and September 13, 2000. A transect consisting of eight sampling points following the flow channel was established from the spring source to 5.6 m downstream (Table 1), at which point the channel merged with flow from other spring sources. At two of the sampling locations (4.4 and 5.0 m), analyses were routinely conducted in duplicate. Relative standard deviations (RSD) between duplicate samples were 5.5% for As(V), 0.7% for total soluble As (As(ts)), less than 1.5% for SO$_4^{2-}$ and major metals, and 31% for sulfide. The high RSD for sulfide at 4.4 and 5.0 m was due only to the fact that sulfide concentrations for these sample locations were often near the reported detection limit (3 μM) for the analytical procedure used in this study (15, discussed below); at higher sulfide concentrations, duplicate samples read normally within 5%. Table 1 reports travel times and water temperatures on November 16, 1999, when most of the reported in situ measurements were conducted. To determine spring water travel times, a spatula was used to bring fine-grained sediments covering the spring bottom into suspension; the reported velocities and travel times were based on the times required for the front of these suspended particulates to travel between individual sampling points in the spring. The velocities were variable throughout the spring transect in response to the fluvial characteristics of the spring; this was especially noticeable from 2.7 to 3.7 m where higher velocities were due to a narrower section of the spring channel. Spring water temperatures and temperature-compensated pH were measured on site using a Mettler Toledo MA130 portable pH meter equipped with a Mettler Toledo IP67 NTC electrode and calibrated using buffers at pH 1.68 and pH 4.01.

Aqueous samples were withdrawn from transect locations using a 20-mL syringe and immediately (<10−20 s) split into three subsamples. For total dissolved sulfide, a 7.5-mL subsample was filtered (0.22 μm) into a test tube containing 0.5 mL of diamine sulfuric acid reagent; 4 drops of FeCl$_3$ reagent were added followed by 1.6 mL of (NH$_4$)$_2$PO$_4$ reagent after 5 min (modified after ref 15). Spectrophotometric analysis was performed in the laboratory within 30 h of sampling, after verifying the stability of the blue complex over at least 2 days. A second aliquot (5 mL) was filtered into a 15-mL HDPE plastic bottle, acidified with 0.1 mL of 12.1 M HCl, and immediately purged with N$_2$(g) for 6 min to remove dissolved sulfide, using a customized portable N$_2$(g) sparging apparatus for field applications. This sample was analyzed for As(ts) using hydride generation atomic absorption spectrometry (HG-AAS; 16), and for S, Na, K, Ca, Mg, Fe,

and Al using inductively coupled plasma emission spectrometry (ICP-ES). The concentrations of total dissolved S in the acidified and purged samples were shown to equal the levels of dissolved SO$_4^{2-}$ in selected samples analyzed using ion chromatography. A third aliquot of each spring water sample was prepared on site for the determination of aqueous As(V) by filtering 5 mL into a 15-mL HDPE bottle containing 1 mL of 2 M Tris buffer (pH 6). While sparging the mixture with N$_2$(g), 1 mL of 0.25 M NaOH and 0.79 M NaBH$_4$ was added in 0.2-mL increments over 4 min to reduce As(III) to arsine gas. The mixture was N$_2$(g) sparged for an additional 3 min to purge arsine. This sample was then preserved in 0.1 M HCl prior to As(V) analysis using HG-AAS. Concentrations of As(III) were determined by difference between As(ts) and As(V) based on previously reported analytical protocols for determining As(V) and As(III) (16). Separate samples were collected for immediate, on-site analysis of total soluble Fe (Fe(ts)) and Fe(II) using the colorimetric FerroZine method (17). In addition, samples for analysis of total dissolved C (TC) were obtained by transferring spring water into glass serum bottles, which were immediately capped with zero headspace to minimize degassing of CO$_2$. For analysis of dissolved organic C (DOC), water samples were acidified to 60 mM H$_3$PO$_4$ and sparged with N$_2$(g) for 6 min. A DC-80 carbon analyzer (Tekmar-Dohrmann, Cincinnati, OH) was used to determine TC and DOC, and dissolved inorganic C (DIC) was calculated as the difference between TC and DOC.

Saturation indices (log(ion activity product/solubility product)) for amorphous As$_2$S$_3$ were calculated with the aqueous equilibrium model, MINTEQA2 (18) utilizing thermodynamic data proposed by Eary (19) for the solubility of As$_2$S$_3$ at 60 °C. Important equilibrium reactions and aqueous complexes of As(III) in Eary's model are

$$0.5As_2S_3(s) + 3H_2O = H_3AsO_3^0 + 1.5H_2S(aq)$$
$$\log K = -10.2$$

$$1.5As_2S_3(s) + 1.5H_2S(aq) = H_2As_3S_6^- + H^+$$
$$\log K = -4.9$$
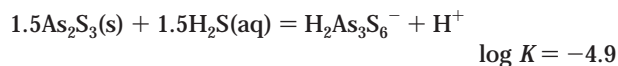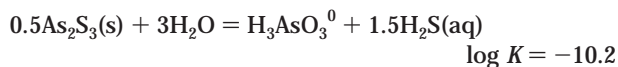
where values of log K are referenced at 60 °C. Newer evidence (20, 21) suggests the existence of at least one additional complex, AsS(OH)(SH)$^-$; however, model predictions of overall As$_2$S$_3$ solubilities were insensitive to the inclusion of this thioarsenite complex at pH $\approx$3 (25 °C), and the temperature dependence of this species has not been investigated. Nevertheless, the recent work (20, 21) on As−S complexation suggests that further improvements will be made in our understanding of important aqueous species of As.

Ex Situ As(III) Oxidation Assays. Abiotic and biotic contributions to the rates of As(III) oxidation were evaluated on site in the presence and absence of both live and killed microbial mat samples. Cores (3.5 cm^2 by 0.5 cm depth) from individual microbial mat zones were transferred to 30-mL wide-mouth HDPE bottles and covered with 3.75 mL of 37% formaldehyde (killed controls with mat only), before adding 30 mL of spring water obtained from the beginning of the brown mat zone (4.4 m). Sample bottles were incubated in a neighboring hot spring of similar temperature (48 °C). Subsamples (1 mL) were taken at 0, 1, 3, and 9 min; filtered using disposable in-line 0.22-μm filters; and analyzed for As(V) or As(ts) as described above.

Rate constants describing the oxidation of As(III) observed in both ex situ and in situ assays were estimated using a least-squares fitting routine assuming a first-order disappearance rate of As(III): [As(III)] = [As(III)]$_0$e^{-kt}, where [As(III)] is the concentration of As(III) in μM, [As(III)]$_0$ is the initial As(III) concentration, t is time in min, and k is the first-order oxidation rate constant in min^{-1}.
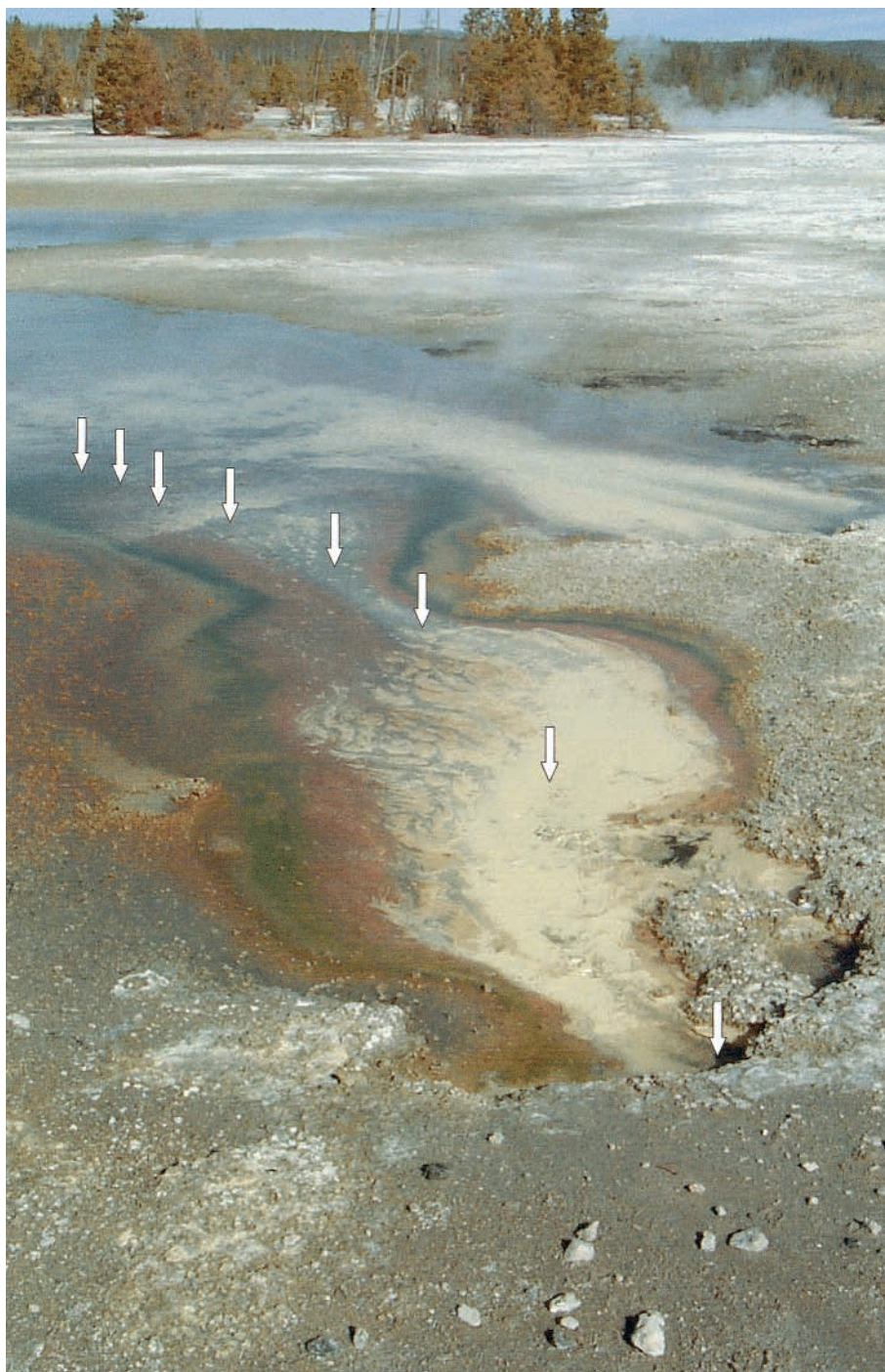
FIGURE 1. Subject geothermal spring located in Norris Basin, YNP, showing sampling locations commencing at the spring source (0 m, 63 °C) and continuing to the center of the green algal mat at 5.6 m (46–48 °C). The sequence of distinct microbial mats occurs in both lateral and longitudinal directions and is typical of many acid–sulfate–chloride thermal springs in YNP. Photograph taken October 20, 1999.

Solid-Phase Characterization. Mat samples corresponding to the primary zones observed in the thermal spring from 0 to 5.6 m were placed in 30-mL vessels, covered with corresponding spring water to achieve zero headspace, and transported to our laboratory. Within 12 h, subsamples of mat material were placed on graphite-coated Al stubs and coated with either Au or C for analysis using a cryostage scanning electron microscope (JEOL 6100) equipped with an energy-dispersive X-ray spectrometer (SEM/EDS). Additional samples of the brown mat were placed on 4-cm² Si wafers and analyzed using an X-ray photoelectron spectroscope (XPS) equipped with a cryostage (PHI model 5600ci). The samples were brought to −134 °C using the cyrostage

to preserve biological integrity and kept under vacuum ($<7 \times 10^{-8}$ Pa) during analysis. Survey and narrow scans were obtained using an Al X-ray source (1486.6 eV) at a constant pass energy of 58.7 V, using a spot size of 400 μm diameter. Charge compensation was employed using the C 1s peak of 284.5 eV as a reference, and all peak positions and areas were calculated using spectral analysis software. Numerous narrow scans were obtained over 10 or 20 eV windows for the following photoelectrons and their respective reference binding energies: Fe2p3/2 (710 eV), As2p3/2 (1324 eV), As3d5/2 (42 eV) S2p (163 eV), N1s (399 eV) Si2s (153 eV), and O1s (532 eV). Total Fe and As contents of mat samples were determined by extraction with 12.1 M HCl for 12 h

TABLE 2. Concentrations of Aqueous Components[a,b] in the Representative Acid–Sulfate–Chloride Thermal Spring within Norris Basin, YNP, Sampled at the Point of Discharge

major ions		weak acids	
ion	concn (mM)	acid	concn (mM)
Na^+	16.3	Si	4.5
K^+	1.2	B	0.9
H^+	0.9[c]	DIC[d]	4.4
Cl^-	16.0	DOC[e]	0.08
SO_4^{2-}	1.3	S(−II)	0.063
		As(III)	0.033

[a] Concentrations of additional detectable constituents (all values in μM): Al (180), Ca (150), Fe(II) (60), Zn (16), Mg (10), Ba (2), Mn (0.9), Sr (0.6), NH$_4$ (70). [b] Undetectable trace elements and method detection limits: P, Se, Ag (<10 μM); Tl, Sb, Pb, Cr, Co, Sn, Ni, Mo, Ti (<1 μM); V, Cd, Cu, Zr, La, Y, Sc, Mn, Yb, Be (<0.1 μM). [c] Based on H^+ activity of 0.79 mM (pH 3.1) and an estimated activity coefficient of 0.87 (Davies equation, 60 °C). [d] Dissolved inorganic C. [e] Dissolved organic C.

followed by analysis of filtered (0.22 μm) extracts using ICP-ES. Ratios of As(III):As(V) in the solid phases were also estimated by on-site extraction using 1 M NaOH (70 °C, 1.5 h) in N_2(g)-purged serum bottles (22). Following extraction, two 1.2-mL aliquots were removed from each serum bottle, neutralized with HCl, diluted to 5 mL, and analyzed for As(V) and As(ts) as described above.

Results and Discussion

Aqueous Chemistry of Thermal Spring. The colorful spring chosen for this study is representative of acid–sulfate–chloride springs common within Norris Basin, YNP. Spring discharge rates often vary annually with higher rates generally observed in the fall (23). The majority of the data presented in this study were collected during a period of relatively high flow between November 1999 and January 2000 when the source water temperature was 63 °C; however, we have observed fluctuations in source water temperature ranging from 58 to 63 °C over the course of a year. More importantly, the water temperature declines in both longitudinal and lateral directions, which is in part responsible for the dramatic biological zonation observed within 6 m of the spring source (Figure 1, Table 1). The predominant chemical constituents of the source water are given in Table 2 and were found to be essentially constant for the sampling events described in the current study (October 1999–June 2000). The primary cations and anions were Na^+, K^+, H^+, Cl^-, and SO_4^{2-}, yielding an ionic strength of approximately 0.02. The source water also contained significant concentrations of sulfide (predominantly H_2S(aq) at a pH of 3.1); As, Si, DIC (4.4 mM); and DOC (80 μM). With the exception of As, concentrations of other trace elements were below levels considered toxic to biota in natural waters (Table 2).

During one of the sampling trips (November 16, 1999), aqueous samples were taken at each transect location five times within a 24-h period and analyzed for temperature, pH, Fe(ts), Fe(II), sulfide, sulfate, As(V), and As(ts). The concentrations of several constituents changed dramatically across the sampling transect, often corresponding to distinct biological zones observed downstream from the source (Figure 1). Most notably, although As(ts) remained constant at 33 μM from 0 to 5.6 m, ratios of As(V):As(ts) increased significantly from 0.05 at 2.7 m to 0.44 at 5 m (Figure 2), corresponding to sampling locations prior to and within the brown and green mats (4.4–5.6 m). The disappearance of As(III) observed within this stream interval corresponded to a fitted first-order As(III) oxidation rate constant (k) of 1.2 ± 0.08 min^{-1} or an As(III) half-life of 0.58 min, based on measured streamwater residence times and As(III) concentrations between 4.4 and 5.6 m (Figure 2B). The estimated
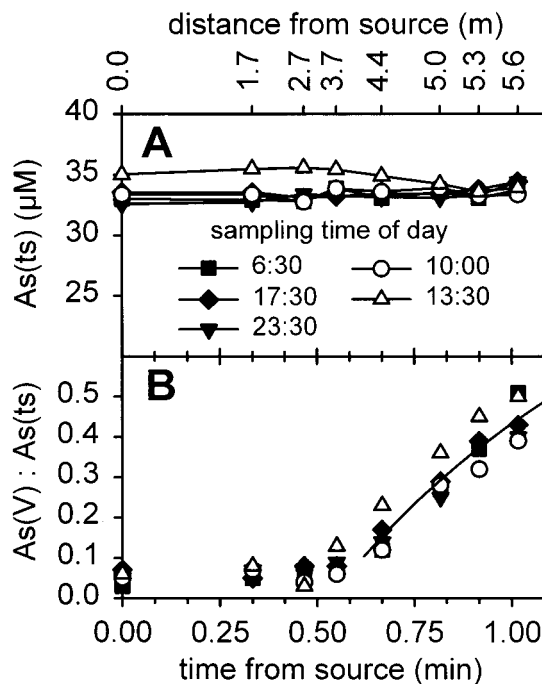
FIGURE 2. Total soluble As (As(ts), panel A) and ratios of As(V): As(ts) (panel B) at five times during the course of a 24-h period (filled symbols, dark samples; open symbols, daylight samples with photon flux densities in the 400–700-nm waveband exceeding 700 μmol s^{-1} m^{-2}). Concentrations are plotted both as a function of travel time (min, bottom x-axis) and as a function of distance (m, top x-axis) from the spring origin. The line in panel B corresponds to the fitted first-order rate equation for As(III) oxidation from 4.4 to 5.6 m, with a rate constant of $k = 1.2 \pm 0.08$ min^{-1} (half-life of 0.58 min). Data were obtained during the November 16, 1999, sampling trip.

rate constant for in situ As(III) oxidation is dependent on flow velocities, which were measured based on suspended particle travel times between sampling points. Although slower overall velocities may be possible as a result of slow flow near water–sediment or water–mat interfaces, a 3-fold longer residence time between 4.4 and 5.6 m would still yield a rate constant of $k = 0.4$ min^{-1} or half-lives <2 min for the oxidation of As(III). Even this conservative estimate represents, to our knowledge, the fastest rate of As(III) oxidation reported for natural water systems. Ratios of As(V):As(ts) measured within the 4–5.6-m stream interval were independent of the time of sampling over a 24-h period (Figure 2), showing that the oxidation of As(III) in this thermal spring was not dependent on abiotic photochemical processes or photosynthetic activity.

Concentrations of soluble sulfide declined from roughly 70 μM at the spring origin to below 7 μM at 4.4 m. The disappearance of sulfide may be partly due to the degassing of H_2S(g), since sulfide exists predominantly as H_2S(aq) at pH <7. In addition, characterization of solid phases present in the yellow mat (discussed below) provided evidence for the accumulation of elemental S, which may arise from rapid sulfide oxidation (24). It is difficult to conclude whether oxidation of reduced S species (H_2S, S^0) resulted in the formation of SO_4^{2-} because the concentrations of SO_4^{2-} at the source were nearly 20-fold higher than concentrations of dissolved sulfide and did not increase substantially over 0–5.6 m (Figure 3F). During one sampling trip (June 2000), the concentrations of thiosulfate were determined on site using ion chromatography and found to be below 0.9 μM throughout the sampling transect (R. B. McCleskey, D. K. Nordstrom, and J. W. Ball, USGS, written communication). Concentrations of dissolved Fe remained constant at 60 μM
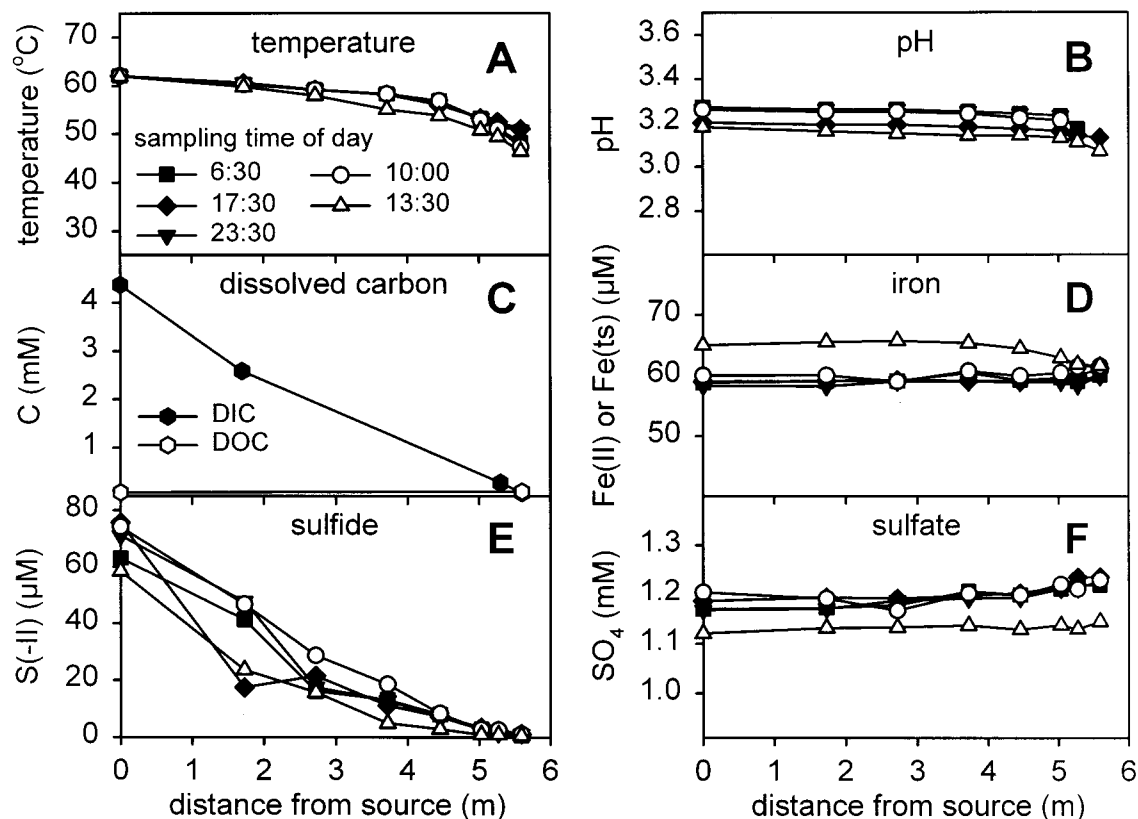
FIGURE 3. Selected aqueous geochemical data along the thermal spring transect obtained during the November 16, 1999, sampling trip. With the exception of dissolved C (panel C), samples from each transect position were obtained five times during the course of a 24-h period. Aqueous Fe(II) and Fe(ts) concentrations were essentially identical (panel D).

from 0 to 5.6 m, and the majority (>99%) of total soluble Fe was Fe(II) at all sampling sites. Similar to that observed for soluble As, we did not detect any diel effects on concentration profiles of sulfide/sulfate, Fe(II)/Fe(III), or pH throughout the spring, suggesting that photochemical processes did not play an important role in controlling the relative concentrations of oxidized and reduced species. The concentration of DIC decreased from approximately 4.4 mM C at the source to 0.07 mM by 5.6 m (Figure 3C). DOC concentrations increased slightly from 0.074 at the source to 0.097 mM by 5.6 m. The loss of DIC may be due both to degassing of CO_2 and to fixation of CO_2 via autotrophic microorganisms.

Biotic Origin of As(III) Oxidation. The role of biotic and abiotic As(III) oxidation pathways was evaluated using ex situ assays performed on site. No oxidation of As(III) was observed in filtered (0.2 μm) spring water with or without formaldehyde over a 9-min assay, confirming that As(III) oxidation rates due to O_2 or other electron acceptors in the aqueous phase were not significant as compared to time scales of oxidation occurring in situ (Figure 4A). Similarly, no oxidation of aqueous As(III) was observed in the presence of yellow mat with or without formaldehyde (not shown). The presence of aqueous sulfide in this zone may preclude significant rates of As(III) oxidation given that As(III) would be thermodynamically favored and that the rate of abiotic reduction of As(V) is known to be significant in the presence of sulfide at low pH (21). However, ex situ assays conducted in the presence of sediment collected at 4.2 m just prior to the brown mat (Figure 4B) and within the brown mat (Figure 4C) showed significant rates of As(III) oxidation ($k = 0.023$ and 0.046 min^{-1}, respectively), corresponding to As(III) half-lives of 31 and 15 min. These results obtained on January 26, 2000, were confirmed during two additional field trips (June 6, 2000, and September 13, 2000), when similar rates of As(III) oxidation were observed. In contrast, rates of As(III)

oxidation in these samples were insignificant when formaldehyde was used to inhibit biological activity (Figure 4B,C). The oxidation of As(III) was also observed in ex situ assays containing green mat ($k = 0.028$ min^{-1}); again, the oxidation of As(III) was suppressed with the addition of formaldehyde. The rates of As(III) oxidation estimated from ex situ assays were considerably lower than oxidation rates measured in situ, likely due to differences in mixing between transport and batch environments or to disturbance of the mat during transfer to ex situ reaction vessels. Nevertheless, the ex situ assays document that the rapid oxidation of As(III) observed in the thermal spring was due to biological processes associated with specific zones (and potentially specific microbial populations) as a function of distance from the spring origin. Furthermore, the half-life observed here is significantly shorter than the value reported by Wilkie and Hering (11) of 0.3 h for in-stream oxidation in Hot Creek, Sierra Nevada Mountains. The higher As(III) oxidation rates observed in the current study may be due to the high microbial biomass:solution ratio of this shallow (<1−2 cm over brown and green mats) and slower flowing spring (0.05− 0.2 m s^{-1} as compared to 0.4 m s^{-1}; ref 11).

Characterization of Microbial Mats. The rapid changes in aqueous geochemistry observed within 6 m of the spring source are coupled with the zonation of biological mats inhabiting the thermal spring. Consequently, mat samples of the prominent zones were further characterized using a complement of analytical techniques to elucidate processes responsible for the biogeochemical cycling of As in the spring interval from 0 to 5.6 m.

The spring is dominated by a yellow mat from 0 to 2.7 m (Figures 1 and 5) that consists of filamentous microorganisms (diameter ≈1 μm) in association with chains of well-crystalline, rhombohedral S^0 (Figure 5B). X-ray diffraction (XRD) peaks of solid phase from this zone exhibit an excellent
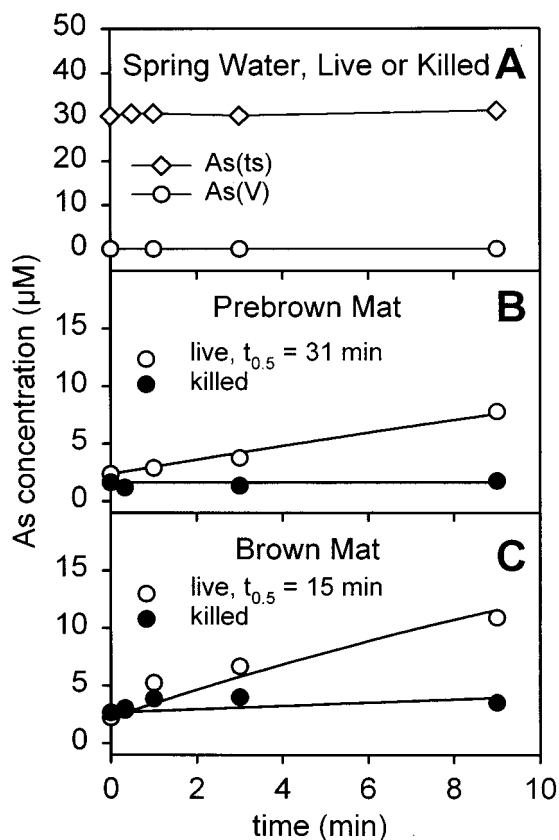
FIGURE 4. Concentrations of As(ts) and As(V) measured during ex situ assays containing filtered spring water (always from 4.4 m in ex situ assays) (A), spring water plus sediment obtained just prior to brown mat (B), and spring water plus brown mat (C) in the presence (closed circles) and absence (open circles) of formaldehyde used to suppress microbial activity. Data presented here comes from assays conducted on site on January 26, 2000, incubated at 48 °C. Fitted lines and estimated half-lives assume a first-order rate expression for the oxidation of As(III). Oxidation rates of As(III) as a function of time in the presence of formaldehyde (killed treatments) are not statistically different than zero, indicating insignificant As(III) oxidation when microbial activity is suppressed.

match to S^0 (JCPDS Card 8-247), and EDS spectra show that the yellow mat consists primarily of S with no detectable As or Fe (Figure 5C). The S^0 solid phase and associated microbial population(s) characteristic of this zone terminate at approximately 2.7 m, consistent with declining aqueous sulfide concentrations (Figure 3E). Upon oxygenation of spring water, H_2S is expected to undergo rapid abiotic oxidation to S^0 and thiosulfate (24). Thiosulfate may disproportionate rapidly to form more S^0 and sulfite (24), which is also extremely labile and would not be expected to accumulate to significant concentrations (24, 25). Consequently, the formation of S^0 in the yellow mat may be entirely abiotic. If so, the S^0 chains associated with the filamentous microbial population(s) may reflect nucleation and crystal growth of S^0 at or along filamentous structures. However, we cannot rule out the possibility that chemolithoautotrophic microorganisms present in the yellow mat are oxidizing $H_2S(aq)$ to form S^0. Furthermore, S^0 and/or SO_4^{2-} (1.2 mM in source water) may serve as electron acceptors for heterotrophic metabolism in this zone.

Interestingly, despite the high levels of As(III) in the source water, no As—S solid phases were observed in the yellow mat (Figure 5C). Thermodynamic calculations based on aqueous chemical modeling and the solubility data of Eary (19) at 60 °C suggest that the spring source water is slightly undersaturated with respect to amorphous As_2S_3 (saturation

index $= -0.8$), but close to saturation with respect to As_2S_3(orpiment) based on interpolation of solubility data from Webster (26) at 25 and 90 °C. We may therefore speculate that As—S solid phases are present at some point in the underground reservoir supplying geothermal water to this spring. Since a complete thermodynamic model accounting for all possible complexes of As(V) and As(III) is not yet available (19–21), the saturation states of the system with respect to amorphous or crystalline As_2S_3 may not be entirely accurate. Regardless, direct evidence from chemical characterization of the yellow mat shows that neither As(III) or As(V) is sequestered within this zone; the rapid disappearance of dissolved sulfide coupled with temperatures that remain near 58 °C throughout the yellow mat preclude the formation of As—S solid phases. Furthermore, the lack of net As(III) oxidation in the yellow zone may be due to several factors including (i) inhibitory effects of sulfide on As-oxidizing microbial populations, (ii) preferential use of reduced S as an electron donor for microbial metabolism as compared to As(III), and (iii) inability to measure As(V) accumulation due to the presence of H_2S, which has been shown to reduce As(V) to As(III) at relatively rapid rates at pH 4 (12, 21).

SEM micrographs of the brown mat reveal an extensive network of filamentous microorganisms (diameter $\approx 1 \mu m$) with a high degree of surface roughness (Figure 5D). However, in contrast to the yellow mat, EDS spectra showed that the brown mat contained virtually no S and is dominated by Fe and As, with As:Fe molar ratios of 0.74 ± 0.02 (Figure 5E). The Fe/As-rich solid phase was amorphous to XRD, suggesting that this mat contains no well-crystalline phases such as goethite, hematite, magnetite, or scorodite ($FeAsO_4 \cdot 2H_2O$). However, several lines of evidence suggest that this phase is an amorphous iron(III) oxyhydroxide containing sorbed As-(V). The oxidation states of Fe and As in this phase were evaluated using X-ray photoelectron spectroscopy (XPS) and extraction with NaOH under anaerobic conditions to prevent the oxidation of As(III) (22). Results from XPS analysis give an Fe 2p3/2 peak position of 712.5 eV, characteristic of Fe-(III) as opposed to Fe(II), which generally shows peak positions of 709–710 eV (27). In addition, the peak position of the As 3d5/2 photoelectron was 45.2 eV, which is consistent with a more oxidized form of As such as Na_2HAsO_4 as suggested by Soma et al. (28). The oxidation state information attainable using XPS is not definitive, but for both Fe and As, the spectra strongly support the more oxidized forms, specifically Fe(III) and As(V). Furthermore, extraction of the solid phase with NaOH under anaerobic conditions followed by analysis of the supernatant showed that all of the desorbable As was As(V). Finally, the reddish-brown color of this solid phase is characteristic of iron(III) oxyhydroxides, unlike scorodite, which is often white to pale green (29). The ratios of As:Fe determined using total dissolution were 0.65, in agreement with EDS data of 0.74 but lower than that expected for scorodite.

Interestingly, the As:Fe ratios observed in the brown mat are consistent with values of 0.68 reported by Waychunas et al. (30) for the surface saturation level of 2-line ferrihydrite coprecipitated with As(V). These authors suggested that high arsenate loading resulted in significant disorder of the iron-(III) hydroxide precipitate, favoring small crystallites of 4–10 Fe(III) octahedra (31), with As(V) tetrahedra forming bidentate binuclear complexes (30, 31). Although there has been some disagreement regarding the EXAFS-derived As—Fe distances and corresponding assignment of specific As—surface complexes on ferrihydrite (32, 33), it is clear that high As loading retards particle growth and slows the rate of transformation of ferrihydrite to more crystalline iron oxides such as hematite. Given the fact that solid-phase As was determined to be primarily As(V) within the brown mat, our results are consistent with sorption of As(V) and saturation of iron oxide
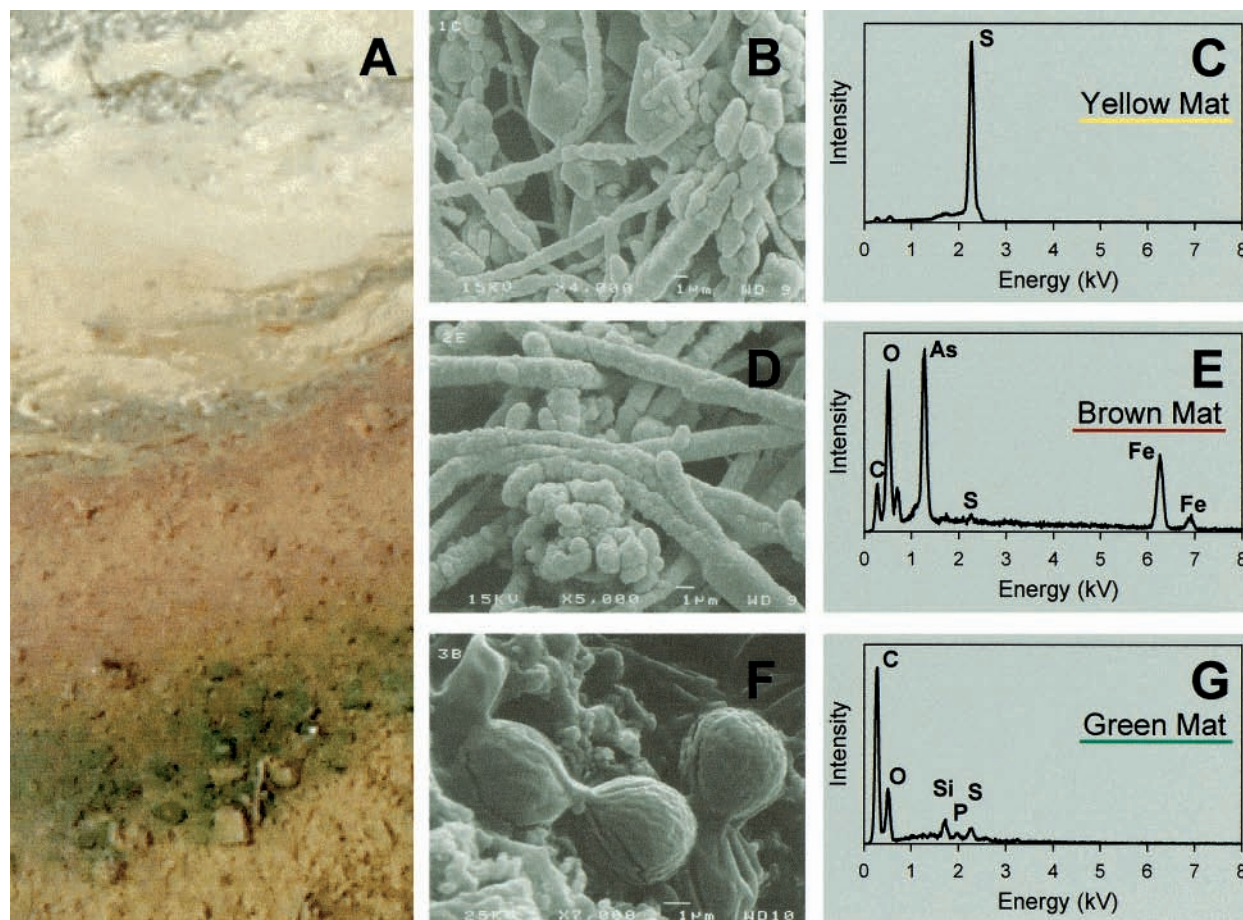
FIGURE 5. Scanning electron micrographs (cryostage) and energy-dispersive X-ray analysis (SEM/EDS) of mat samples representing the predominant biogeochemical zones in the acidic geothermal spring. Yellow, brown, and green mat sections are shown extending laterally from the flow direction (panel A); rhombohedral structures of S^0 and filamentous microorganims (1 μm diameter) coexist in the yellow mat (panel B); and EDS confirms the dominance of S^0 (panel C). Microbial filaments (1 μm diameter) in the brown mat (panel D) show solid-phase coatings consisting primarily of As and Fe (panel E) at a molar As:Fe ratio of 0.7. The surface of the green mat (panel F) is dominated by algal cells (presumably *Cyanidium)*, but the EDS spectra of this zone may or may not (as shown in panel G) exhibit the presence of As and Fe, depending on the density of algal cells.

surface sites during the precipitation of the Fe-rich phase. The fact that this phase is amorphous to XRD appears consistent with the effects of high As on the order and crystal growth of iron oxides.

The mechanism responsible for the oxidation of Fe(II) to form an iron(III) hydroxide phase has not been determined but likely is due to microbiological processes because it has been shown in other studies that the abiotic oxidation of Fe(II) to Fe(III) is extremely slow at low pH (*13, 34*). Furthermore, tentative identification of an Fe(II)-oxidizing organism in the brown mat (*14*) supports this hypothesis. The fact that aqueous Fe is dominated by Fe(II) throughout the spring transect indicates that the rate of Fe(II) actually oxidized is much lower than the total flux of Fe(II) from the spring source. Consequently, it was not possible to use changes in aqueous Fe concentrations as a method for estimating the deposition rate of iron(III) hydroxides in the brown mat; the time required for the formation of the brown, Fe-rich mats observed in this and similar acid−sulfate−chloride thermal springs is not currently known.

High rates of As(III) oxidation extended into the green mat (starting at 5.3 m) characterized by a dense surface coverage of algal cells (diameter ≈5 μm, Figure 5F) consistent with the morphology and temperature range of *Cyanidium caldarium*, which has been previously identified to be associated with low pH, thermal springs in YNP (*35*). The boundary between brown and green mats was not abrupt,

and the distribution of algal cells was often discontinuous within this transition. These observations were confirmed using SEM/EDS. For example, in some cases, EDS analyses of the green zone showed significant concentrations of Fe and As with As:Fe ratios identical to values observed in the brown mat. In other cases, the only elements observed with EDS were C, O, and Si, suggesting a denser coverage of algal cells on Si-rich solid phases without Fe and As (Figure 5G). The algal population observed in the 45−51 °C temperature zone was subject to seasonal variation and was visibly absent during the summer months (June−September) before reoccurring in the fall (October−November). Identical As(III) oxidation patterns were observed during the June sampling trip in the absence of a visible algal population, suggesting that the algal population does not contribute significantly to the high rates of As(III) oxidation measured in situ.

Microbial Community Structure and Mechanisms of As(III) Oxidation. Although our results show that the rapid oxidation of As(III) in this thermal spring is biologically mediated, we cannot at this time assign a specific microbial population or mechanistic pathway responsible for the oxidation of As(III). Known mechanisms of As(III) oxidation by microorganisms include chemolithoautotrophic metabolism where As(III) is used as an energy source (*4*) and extracellular oxidation of As(III) via an arsenite oxidase as observed in *Alcaligenes* sp. (*8*). We have more fully characterized the microbial populations present in the prominent

geochemical zones observed in this thermal spring in a companion study (*14*). Briefly, results from Jackson et al. (*14*) suggest the presence of similar bacterial populations in both yellow and brown mats and the presence of several archaeal populations confined to the brown mat. Approximately 90% of the bacterial (16S rDNA PCR cloned) DNA sequences obtained from both yellow and brown zones belong to organisms similar to *Hydrogenobacter acidophilus* (H_2 or S^0 oxidizing bacterium) and *Desulfurella* sp. (S^0 reducer), whereas the archaeal sequences obtained have no cultured relatives. There are no reports in the literature regarding the ability of *Hydrogenobacter* sp. or *Desulfurella* sp. to oxidize As(III). Consequently, we have initiated enrichment experiments to definitively link specific microbial populations present in the spring with the observed As(III) oxidation rates. Microbial pathways responsible for the oxidation of As(III) in high As thermal environments may represent early evolutionary traits that are distributed in other water and soil microorganisms. The ability of microorganisms to oxidize As(III) has important implications in the biogeochemical cycling of As, in part due to the often reported lower toxicity of As(V) versus As(III). Furthermore, the production of As(V) can result in the subsequent selection of microorganisms capable of utilizing As(V) as a terminal electron acceptor during anaerobic growth perpetuating transformation among As(III) and As(V). In general, the high concentrations of As in thermal springs of YNP provide an excellent opportunity to study the evolution of metabolic traits associated with As transformations in natural water systems.

Acknowledgments

Literature Cited

(1) Ball, J. W.; Nordstrom, D. K.; Cunningham, K. M.; Schoonen, M. A. A.; Xu, Y.; DeMonge, J. M. Water-chemisty and on-site sulfur-speciation data for selected springs in Yellowstone National Park, Wyoming, 1994−1995; USGS Open File Report 98-574; U.S. Goverment Printing Office: Washington, DC, 1998.

(2) Stauffer, R. E.; Thompson, J. M. *Geochim. Cosmochim. Acta* **1984**, *48*, 2547−2561.

(3) Ilyaletdinov, A. N.; Abdrashitova, S. A. *Mikrobiologiya* **1981**, *50*, 197−204.

(4) Santini, J. M.; Sly, L. I.; Schnagl, R. D.; Macy, J. M. *Appl. Environ. Microbiol.* **2000**, *66*, 92−97.

(5) Stolz, J. F.; Oremland, R. S. *FEMS Microbiol. Rev.* **1999**, *23*, 615−627.

(6) Cervantes, C.; Ji, G.; Ramirez, J. L.; Silver, S. *FEMS Microbiol. Rev.* **1994**, *15*, 355−367.

(7) Tamaki, S.; Frankenberger, W. T., Jr. *Rev. Environ. Contam. Toxicol.* **1992**, *124*, 79−110.

(8) Anderson, G. L.; Williams, J.; Hille, R. *J. Biol. Chem.* **1992**, *267*, 23674−23682.

(9) Ball, J. W.; Nordstrom, D. K.; Jenne, E. A.; Vivit, D. V. Chemical analysis of hot springs, pools, geysers, and surface waters from Yellowstone National Park, Wyoming, and vicinity, 1974−1975; USGS Open File Report 98-182; U.S. Goverment Printing Office: Washington, DC, 1998.

(10) Stauffer, R. E.; Jenne, E. A.; Ball, J. W. Chemical studies of selected trace elements in hot-spring drainages of Yellowstone National Park; USGS Professional Paper 1044-F; U.S. Goverment Printing Office: Washington, DC, 1980.

(11) Wilkie, J. A.; Hering, J. G. *Environ. Sci. Technol.* **1998**, *32*, 657−662.

(12) Cherry, J. A.; Shaikh, A. U.; Tallman, D. E.; Nicholson, R. V. *J. Hydrol.* **1979**, *43,* 373−392.

(13) Eary, L. E.; Schramke, J. A. In *Chemical Modeling of Aqueous Systems II*; Melchior, D. C., Bassett, R. L., Eds.; American Chemical Society Symposium Series 416; American Chemical Society: Washington, DC, 1990; pp 379−396.

(14) Jackson, C. R.; Langner, H. W.; Donahoe-Christiansen, J.; Inskeep, W. P.; McDermott, T. R. Molecular analysis of microbial community structure in an arsenite oxidizing acidic thermal spring. *Environ. Microbiol.*, in press.

(15) American Public Health Association. Part 4500-S^{2-} D. In *Standard methods for the examination of water and wastewater*, 20th ed.; Clesceri, L. S., Greenberg, A. E., Eaton, A. D., Eds.; APHA: Washington, DC, 1998; pp 4-165−4-166.

(16) Jones, C. A.; Langner, H. W.; Anderson, K.; McDermott, T. R.; Inskeep, W. P. *Soil Sci. Soc. Am. J.* **2000**, *64*, 600−608.

(17) To, T. B.; Nordstrom, D. K.; Cunningham, K. M.; Ball, J. W.; McClesky, R. B. *Environ. Sci. Technol.* **1999**, *33*, 807−813.

(18) Allison, J. D.; Brown, D. S.; Novo-Gradac, K. J. *MINTEQA2/PRODEFA2, a geochemical assessment model for environmental systems: Version 3.0 User's Manual*; U.S. EPA Environmental Research Laboratory, Office of Research and Development: Athens, GA, 1991.

(19) Eary, L. E. *Geochim. Cosmochim. Acta* **1992**, *56*, 2267−2280.

(20) Helz, G. R.; Tossell, J. A.; Charnock, J. M.; Pattrick, R. A. D.; Vaughan, D. J.; Garner, C. D. *Geochim. Cosmochim. Acta* **1995**, *59*, 4591−4604.

(21) Rochette, E. A.; Bostick, B. C.; Li, G.; Fendorf, S. *Environ. Sci. Technol.* **2000**, *34*, 4714−4720.

(22) Langner, H. W.; Inskeep, W. P. *Environ. Sci. Technol.* **2000**, *34*, 3131−3136.

(23) Fournier, R. O.; Thompson, J. M.; Hutchinson, R. A. The geochemistry of hot spring waters at Norris Geyser Basin, Yellowstone National Park, USA. In *Water−Rock Interaction*; Kharaka, Maest, Eds.; Balkema: Rotterdam, 1992; pp 1289−1292.

(24) Xu, Y.; Schoonen, M. A. A.; Nordstrom, D. K.; Cunningham, K. M.; Ball, J. W. *Geochim. Cosmochim. Acta* **1998**, *62*, 3729−3743.

(25) Zangh, J.-Z.; Millero, F. J. Kinetics of oxidation of hydrogen sulfide in natural waters. In *Environmental geochemistry of sulfide oxidation*; Alpers, C. N., Blowes, D. W., Eds.; American Chemical Society: Washington, DC, 1994; pp 393−409.

(26) Webster, J. G. *Geochim. Cosmochim. Acta* **1990**, *54*, 1009−1017.

(27) Moulder, J. F.; Stickle, W. F.; Sobol, P. E.; Bomben, K. D. *Handbook of X-ray Photoelectron Spectroscopy*; Perkin-Elmer Corporation, Physical Electronics Division: Eden Prairie, MN, 1992.

(28) Soma, M.; Tanaka, A.; Seyama, H.; Satake, K. *Geochim. Cosmochim. Acta* **1994**, *58*, 2743−2745.

(29) Robins, R. G. *Am. Mineral.* **1987**, *72*, 842−844.

(30) Waychunas, G. A.; Rea, B. A.; Fuller, C. C.; Davis, J. A. *Geochim. Cosmochim. Acta* **1993**, *57*, 2251−2269.

(31) Waychunas, G. A.; Fuller, C. C.; Rea, B. A.; Davis, J. A. *Geochim. Cosmochim. Acta* **1996**, *60*, 1765−1781.

(32) Manceau, A. *Geochim. Cosmochim. Acta* **1995**, *59*, 3647−3653.

(33) Waychunas, G. A.; Davis, J. A.; Fuller, C. C. *Geochim. Cosmochim. Acta* **1995**, *59*, 3655−3661.

(34) Nordstrom, D. K.; Southam, G. In *Geomicrobiology: Interactions between microbes and minerals*; Banfield, J. F., Nealson, K. H., Eds.; Reviews in Mineralogy 35 ; Mineralogical Society of America: Washington, DC, 1997; Chapter 11, pp 361−390.

(35) Seckbach, J. In *Evolutionary pathways and enigmatic algae: Cyanidium caldarium (Rhodophyta) and related cells*; Seckbach, J., Ed.; Kluwer Academic Publishers: Dordrecht, The Netherlands, 1994; pp 99−112.